High Pressure Behavior of $Sr_3(VO_4)_2$ and $Ba_3(VO_4)_2$

Andrzej Grzechnik and Paul F. McMillan[1]

Department of Chemistry, Arizona State University, Tempe, Arizona 85287-1604, and Ecole Normale Supérieure de Lyon, 46 allée d'Italie, 69007 Lyon, France

We have studied pressure-induced transitions and structural changes in isostructural strontium and barium orthovanadates, $Sr_3(VO_4)_2$ and $Ba_3(VO_4)_2$, via Raman spectroscopy. The spectral changes in $Ba_3(VO_4)_2$ can be interpreted as being due to condensation of VO_4^{3-} units into edge- or corner-shared octahedra with little or no hysteresis on decompression. For $Sr_3(VO_4)_2$, there is a pressure-induced first-order phase change at about 150 kbar, with large hysteresis on decompression, which can be rationalized as a transition into a spinelloid series of structures, retaining the tetrahedral coordination of the V atoms.

© 1997 Academic Press

INTRODUCTION

The alkaline earth metal orthovanadates, $Me_3(VO_4)_2$ (*Me*: Ca, Sr, Ba), have attracted much attention owing to their interesting optical, transport, and ferroelectric properties [1–7]. Among them, strontium and barium orthovanadates, $Sr_3(VO_4)_2$ and $Ba_3(VO_4)_2$, exhibit intense rare earth activated luminescence and can be used as luminophors and host materials for lasers (1). The intensity of luminescence in $Sr_3(VO_4)_2$ and $Ba_3(VO_4)_2$ can be additionally enhanced through the formation of the $Ca_3(VO_4)_2$–$Sr_3(VO_4)_2$ and $Ca_3(VO_4)_2$–$Ba_3(VO_4)_2$ solid solution series (2). Also, intense luminescence can be obtained by tuning the composition in the solid solution series between the isostructural orthovanadates and orthophosphates (8–11). For that instance, the intensity of luminescence in the system $(Ca, Sr, Y)_3[(V, P)O_4]_2 : Sm^{3+}$ approaches that of commercially used luminophors (1). Recently, near-IR laser action of $Sr_3(VO_4)_2 : Mn^{5+}$ at 1168 nm and $Ba_3(VO_4)_2 : Mn^{5+}$ at 1181 nm has been reported by Merkle *et al.* (3) and Buijsse *et al.* (4).

Further investigations of alkali earth orthovanadates are of interest to possibly develop new series of optical com-pounds. Luminescence in these compounds is largely determined by point defects in the crystal structure. We have recently investigated the use of high pressure in formation of quenchable metastable oxides with the perovskite and lithium niobate structures (12–15). The purpose of the present study is to begin to explore the potential of high pressure methods for preparation of new compounds in the orthovanadate systems. As in our previous studies, it was useful to begin with an investigation of the phase transformations occurring in the pure compounds at high pressure and during their decompression path (12). The phase transitions and structural distortions are conveniently followed by Raman spectroscopy, carried out *in situ* in the diamond anvil cell (16).

EXPERIMENTAL

The polycrystalline samples of $Sr_3(VO_4)_2$ and $Ba_3(VO_4)_2$ were prepared from 3 : 1 mixtures of $SrCO_3$ and V_2O_5, and $BaCO_3$ and V_2O_5 (all from Aldrich) compressed into pellets and heated in 1373 K for 72 h with one additional intermittent grinding. Formation of the compounds was verified by X-ray diffraction ($Sr_3(VO_4)_2$: JCPDS-ICDD No. 29-1318; $Ba_3(VO_4)_2$: JCPDS-ICDD No. 25-1192). Additionally, absence of Ba and Sr pyrovanadates was evidenced by absorbance infrared spectra (1).

Raman spectra were measured in backscattering geometry with an ISA S-3000 triple spectrograph with CCD detection (a Princeton Instruments LN/CCD-1100 detector). The laser focusing and signal collection optics systems were built around a modified BH-2 Olympus microscope. The scattered signal was focused and spatially filtered on the entrance slit of the spectrometer. Raman scattering was excited using the 488.0-nm line of an Ar^+ ion laser (Coherent 90-5). The samples were loaded into a Mao-Bell-type diamond cell with type I diamonds, brilliant cut with 350 μm culets, and a sample chamber diameter of 150 μm. CsI was used as a pressure transmitting medium. Pressures were determined from the shift of the R_1 ruby fluorescence line (17).

---

[1] Foreign Associate, Institut Universitaire de France.

STRUCTURAL DESCRIPTION AND SYMMETRY CONSIDERATIONS

The structure of the whole family of $Me_3(XO_4)_2$ (Me: Sr, Ba; X: P, As, V, Cr, Mn) compounds with $R\bar{3}m$ space group (8–11) can be derived from the structure of $K_2Pb(SO_4)_2$ palmierite (18). It is composed of $[Me_{(1)}(XO_4)_2]^{4-}$ layers linked into a crystal network by $Me_{(2)}^{2+}$ cations (Fig. 1). The VO_4^{3-} groups in strontium and barium orthovanadates occupy C_{3v} sites, but are only slightly distorted from tetrahedral geometry (11, 19). The O–V–O angles range from 109.2 to 109.7° in $Ba_3(VO_4)_2$ and 109.4 to 109.6° in $Sr_3(VO_4)_2$. In both compounds, there are three longer and one shorter V–O distances: 1.707 and 1.698 Å in $Ba_3(VO_4)_2$ and 1.717 and 1.694 Å in $Sr_3(VO_4)_2$. The small departure from tetrahedral geometry makes it useful to correlate the vibrational modes of the VO_4^{3-} groups in these structures with those of the ideal T_d symmetry. The intralayer $Me_{(1)}$

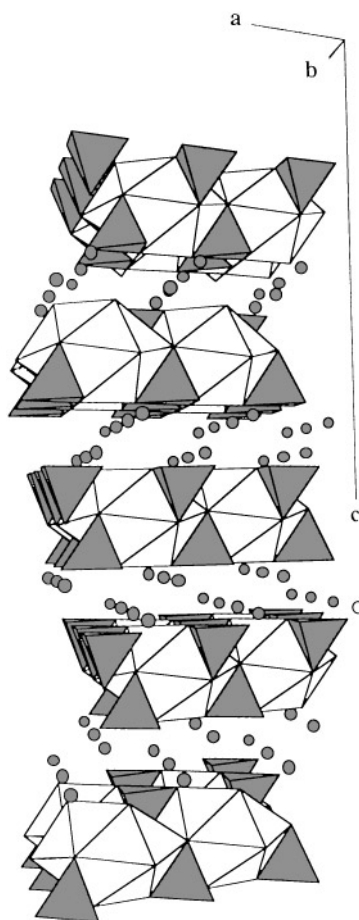**FIG. 1.** Stacking of structural layers in $Me_3(XO_4)_2$ (Me: Sr, Ba; X: V, P, Cr, Mn) along the c axis in a hexagonal setting. The layers are composed of XO_4 tetrahedra and $Me_{(1)}O_{12}$ icosahedra. Between the layers are the $Me_{(2)}$ atoms (filled circles).

cations in these structures occupy D_{3d} symmetry sites which can be described either as octahedral ($6 * Ba–O'$; 2.758 Å; $6 * Sr–O'$; 2.608 Å) or as distorted 12-fold icosahedral coordination polyhedra ($6 * Ba–O'$, 2.758 Å; $6 * Ba–O''$, 3.329 Å; $6 * Sr–O'$, 2.608 Å; $6 * Sr–O''$, 3.252 Å) (11, 19). The coordination number of the interlayer $Me_{(2)}$ atoms is 10 (C_{3v} symmetry sites), with Me–O distances ranging from 2.609 to 2.938 Å ($Ba_3(VO_4)_2$) and 2.405 to 2.872 Å ($Sr_3(VO_4)_2$).

Symmetry analysis gives the normal modes in $Me_3(XO_4)_2$ compounds (D_{3d}^5 space group) as $\Gamma_{vib} = 5A_{1g} + A_{2g} + 6E_g + A_{1u} + 5A_{2u} + 6E_u$, where A_{1g} and E_g modes are Raman active, and A_{2u} and E_u modes are infrared active (16). Internal stretching and bending XO_4^- modes are distributed as $\Gamma_{int} = 3A_{1g} + 3E_g + 3A_{2u} + 3E_u$, whereas the translational and rotational modes are $\Gamma_T = 2A_{1g} + 2E_g + 2A_{2u} + 2E_u$ and $\Gamma_R = A_{2g} + E_g + A_{1u} + E_u$, respectively. The internal modes of an isolated tetrahedral molecule with T_d symmetry (i.e., ideal VO_4^{3-}) are classified as v_1 (the symmetric stretching mode of the A_1 symmetry type), v_2 (the bending mode of the E symmetry type), v_3 (the anti-symmetric stretching mode of the F_2 symmetry type), and v_4 (the bending mode of the F_2 symmetry type). The descent in symmetry to C_{3v} point group for the distorted VO_4^{3-} group in space group D_{3d}^5 leads to removal of threefold degeneracy and causes some mixing between the v_1 and v_3 stretching and the v_2 and v_4 bending modes. Because two VO_4^{3-} groups are vibrationally coupled (related by an inversion centre) within the primitive cell, there are 18 degrees of internal freedom. The modes derived from the v_1, v_2, v_3, and v_4 modes of the ideal tetrahedron have the $A_{1g} + A_{2u}$, $E_g + E_u$, $A_{1g} + E_g + A_{2u} + E_u$, and $A_{1g} + E_g + A_{2u} + E_u$ symmetry types, respectively. We thus expect three high frequency Raman modes ($2A_{1g} + E_g$) derived from v_1 and v_3 stretching motions, and three at lower frequency ($A_{1g} + 2E_g$) derived from v_2 and v_4 bending motions.

RESULTS AND DISCUSSION

Assignment of the Room Pressure Spectra

The Raman spectra of $Sr_3(VO_4)_2$ and $Ba_3(VO_4)_2$ taken at ambient conditions are displayed in Fig. 2 and band assignments are summarized in Table 1. The observed Raman bands are distributed in three well-separated frequency regions corresponding to the V–O stretching modes (850–750 cm^{-1}), O–V–O bending modes (450–300 cm^{-1}), and translational and rotational modes of the VO^{3-} groups mixed with the Ba^{2+} or Sr^{2+} displacements (250–120 cm^{-1}) (1). Only two strong peaks are visible in the high frequency region. Our high pressure results (see below) indicate that the lower frequency peak corresponds to one of the A_{1g} modes derived from the v_1 and v_3 tetrahedral stretching vibrations, and that the higher frequency band contains both the E_g mode derived from v_3 and the remaining A_{1g} mode. It is likely
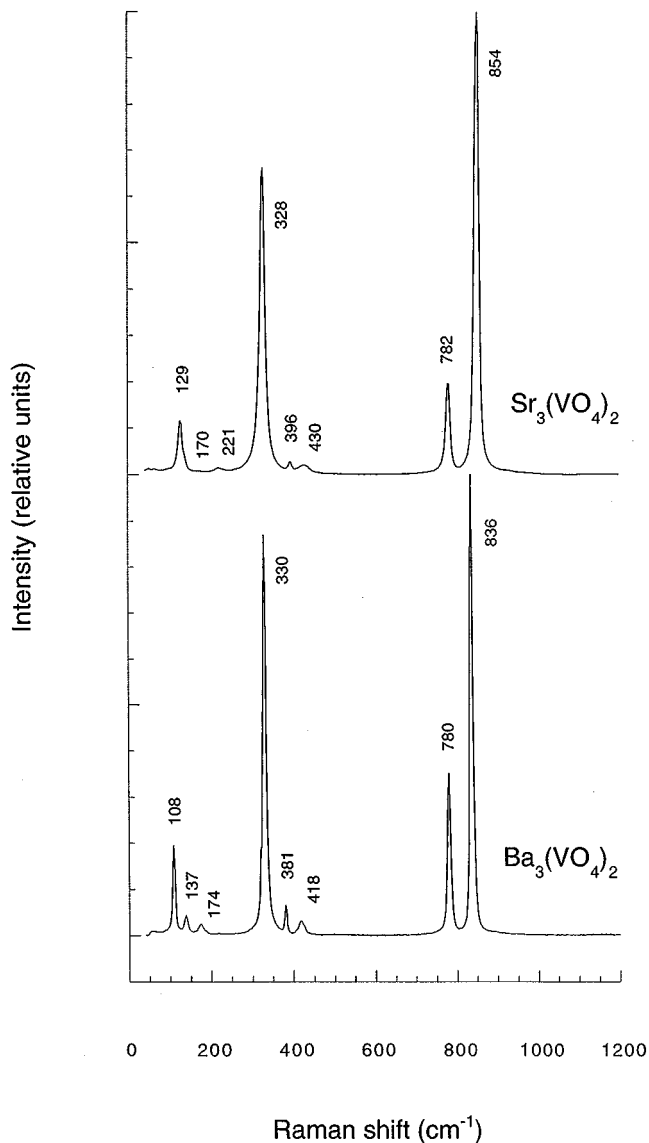
$Sr_3(VO_4)_2$	$Ba_3(VO_4)_2$	Assignment
854	836	v_1, v_3
782	780	v_3
430	418	v_2
396	381	v_4
328	330	v_4
221	174	$T(Me_{(2)}) + T(VO_4^{3-})$
170	137	$T(Me_{(2)}) + R(VO_4^{3-})$
129	108	$T(Me_{(2)})$

FIG. 2. Raman spectra of $Sr_3(VO_4)_2$ and $Ba_3(VO_4)_2$ at ambient conditions.

that the symmetric breathing and asymmetric stretching motions of the isolated tetrahedron become mixed on descent in symmetry to the C_{3v} site group. The lower frequency A_{1g} mode occurs at the same frequency in both compounds (780, 782 cm^{-1}), but the higher frequency band (which is dominated by the other A_{1g} mode) shifts from 836 cm^{-1} in $Ba_3(VO_4)_2$ to 854 cm^{-1} in $Sr_3(VO_4)_2$. It is quite likely that this vibration has a larger component of V–O stretching of the short V–O bond aligned with the c axis, which decreases slightly in length from the Ba- to the Sr-compound (11, 19). The strong peak at 330 cm^{-1} in both compounds can be identified as the fully symmetric A_{1g} mode derived from v_4 bending, whereas the two weaker

peaks in the 380–430 cm^{-1} region are the E_g modes derived from v_2 and v_4. The width of the Raman peaks in the $Sr_3(VO_4)_2$ spectrum is generally greater than for those in the spectrum of $Ba_3(VO_4)_2$, perhaps reflecting a greater degree of anharmonicity in the more distorted VO_4^{3-} groups.

The lowest frequency peak occurs at 129 cm^{-1} for $Sr_3(VO_4)_2$. This moves to 108 cm^{-1} for $Ba_3(VO_4)_2$, which permits its identification as the mode derived from translation of the $Me_{(2)}^{2+}$ cations. The expected mass shift factor is $\sqrt{(m_{Sr}/m_{Ba})} = 0.801$, compared with 0.837 observed. The same shift is observed for the 221 cm^{-1} peak ($Sr_3(VO_4)_2$) that moves to 174 cm^{-1} for $Ba_3(VO_4)_2$, which allows it to be identified as the mode from the $Me_{(2)}^{2+}$ cation displacements. The vibrations of the $Me_{(1)}^{2+}$ cations do not appear in the Raman spectrum, because they lie on inversion centers. The remaining features in the low frequency region can be assigned to VO_4^{3-} librations and translations. It is likely that these will actually be mixed with the $Me_{(2)}^{2+}$ cation translational modes.

Spectral Changes with Pressure

The spectra obtained *in situ* at high pressure are shown in Figs. 3 and 4, and peak shifts are summarized in Figs. 5(a–d). In the spectra of $Sr_3(VO_4)_2$, the highest frequency band begins to broaden above approximately 20 kbar and has developed a distinct low frequency shoulder by 63 kbar (Fig. 3). For $Ba_3(VO_4)_2$, the second component is resolved as a separate peak maximum as low as 25 kbar (Fig. 4). Our results on compression to higher pressures ($Sr_3(VO_4)_2$; Fig. 3) indicate that this most likely corresponds to the E_g mode derived from the tetrahedral v_3 stretching vibration expected from symmetry analysis, which has a smaller pressure shift than the two A_{1g} modes. On compression above 95 kbar, the central band appears to split into two components, which would be consistent with removal of the degeneracy for the E_g mode. This could be associated with reduction in the symmetry of the VO_4^{3-} units to C_{2h} or lower symmetry, which might occur via
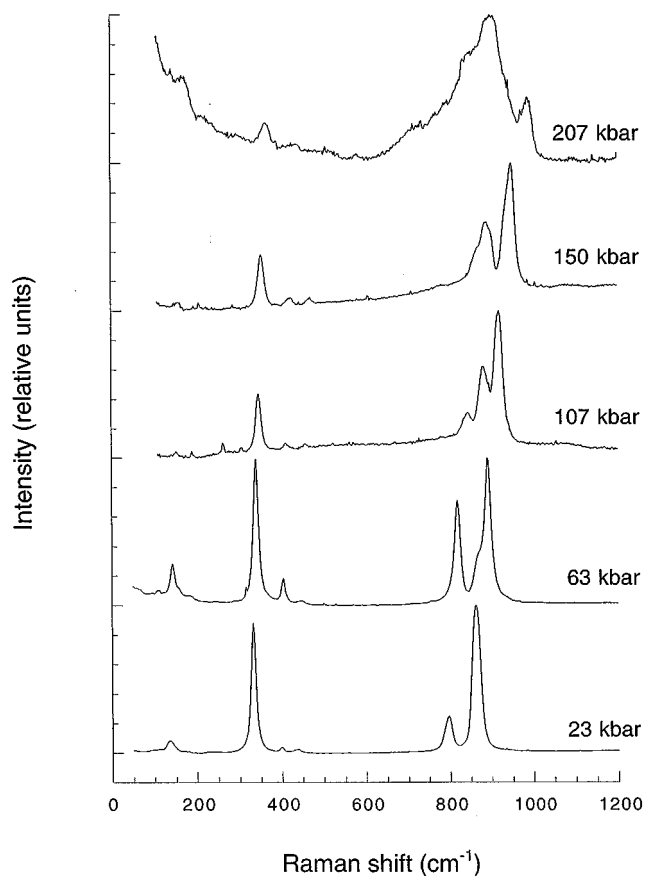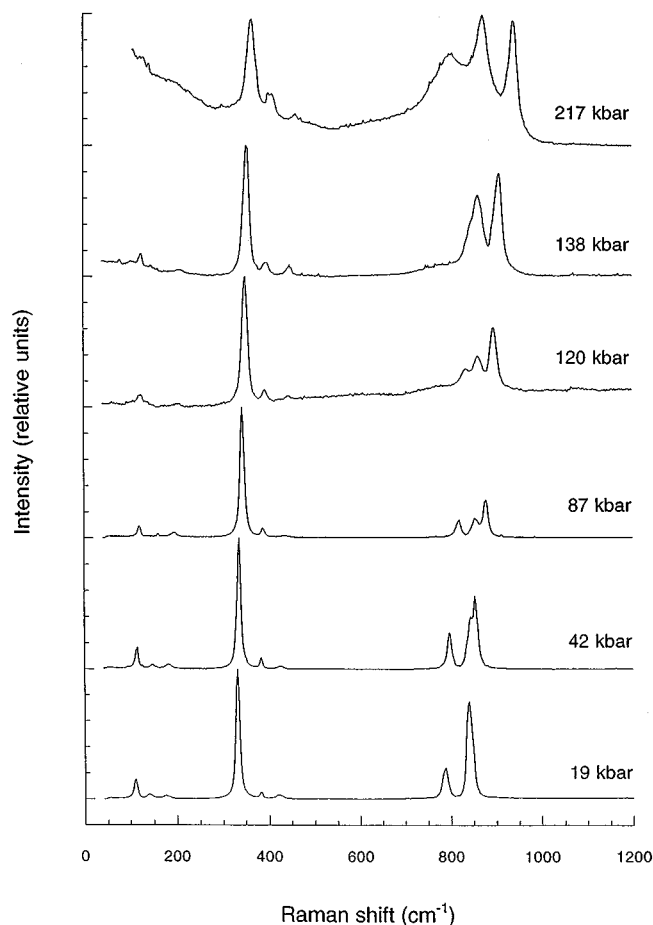
FIG. 3. Raman spectra of $Sr_3(VO_4)_2$ upon compression.

FIG. 4. Raman spectra of $Ba_3(VO_4)_2$ upon compression.

pressure-induced displacements of the $Sr_{(2)}^{2+}$ cations associated with distortion of the vanadate units (loss of the 3-fold axis). The shifts of the $Sr_{(2)}^{2+}$ cations can eventually lead to a largely distorted 10-fold coordinated polyhedra or lower coordination. Because no obvious splitting of the doubly degenerate bending mode in the $300-400 \text{ cm}^{-1}$ region is observed, this suggests that any such distortion would be associated with the V–O bond lengths, rather than the O–V–O angles.

By 140–150 kbar, both lower frequency bands have merged because of their differing pressure shifts (Figs. 3, 4). Above this pressure, radical changes begin to be observed in the spectra, and qualitative differences in behavior appear for the two compounds. In the case of $Sr_3(VO_4)_2$, a strong, broad, asymmetric band centred near 850 cm^{-1} dominates the spectrum, while the high frequency A_{1g} mode of the low-pressure structure remains visible to the highest pressure studied (207 kbar). Very weak broad features are also observed in the $700-750 \text{ cm}^{-1}$ region, which can be distinguished from the baseline at pressures as low as 107 kbar (Fig. 3). On decompression, the strong asymmetric band

dominates the spectrum to 117 kbar (Fig. 6). Below this pressure, the spectrum of the room pressure phase is recovered, but very weak, broad features near $700-750 \text{ cm}^{-1}$ are still visible in the ambient pressure spectrum.

For $Ba_3(VO_4)_2$, the spectrum taken at 156 kbar resembles that for $Sr_3(VO_4)_2$ (150 kbar; Fig. 3), but the broad band near 800 cm^{-1} is much more marked (Fig. 4). By 195 kbar, the $Ba_3(VO_4)_2$ spectrum does generally resemble the $Sr_3(VO_4)_2$ taken in the same pressure range, but the broad feature is much more spread out, and has distinct maxima near 800 and 850 cm^{-1}. At the highest pressure (217 kbar), the spectrum is dominated by two strong peaks at 930 and 860 cm^{-1}, as well as a broader band near 800 cm^{-1}. There is also weak, diffuse scattering in the $600-700$ cm-1 region (Fig. 4). Like $Sr_3(VO_4)_2$, the spectrum of the room pressure phase is recovered below approximately 120 kbar (Fig. 7): however, the spectrum changes much more gradually on decompression than for the strontium orthovanadate, which more or less retains its high pressure band profile until the reversion (Fig. 6).
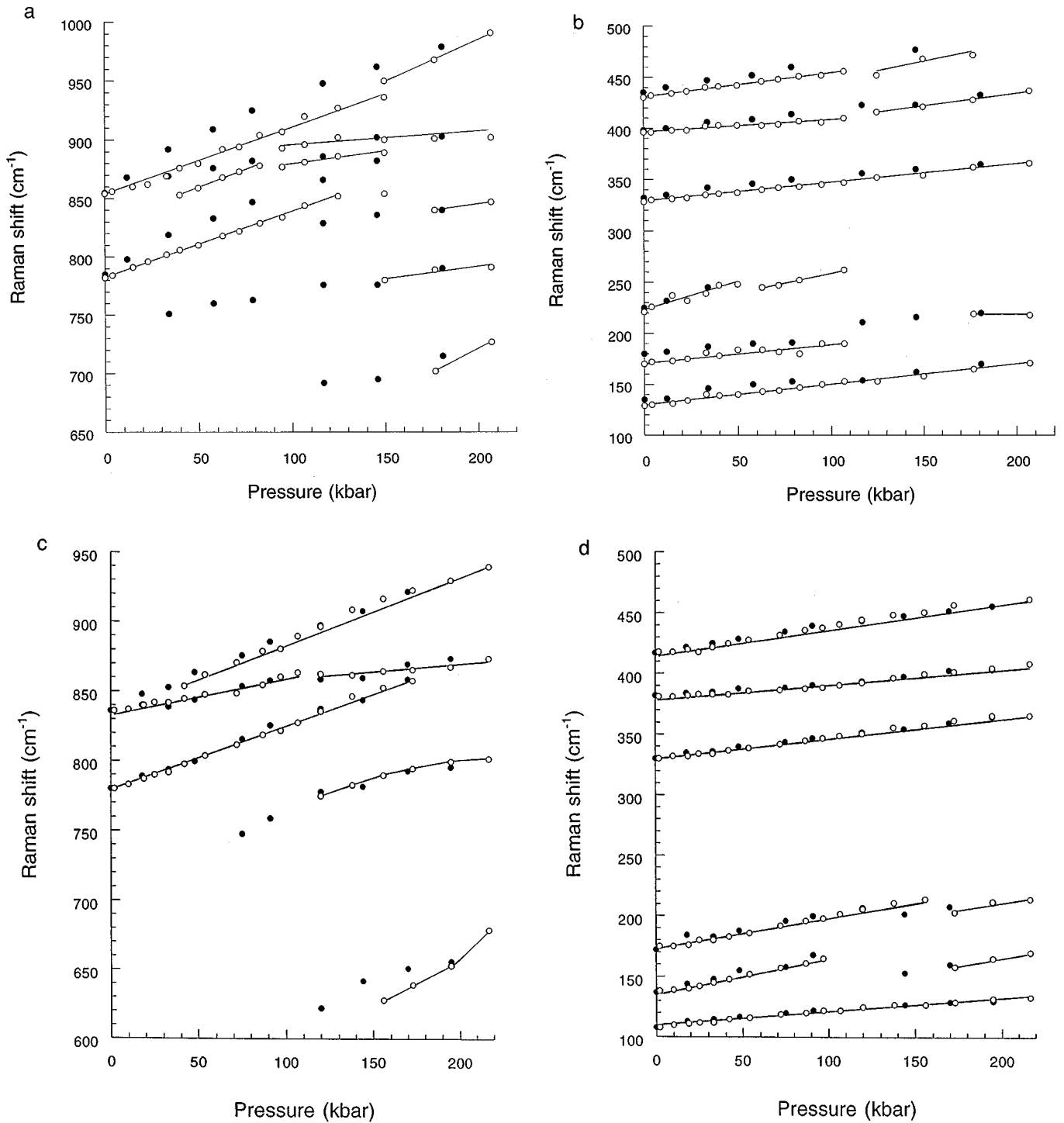
FIG. 5. The pressure shift of the Raman bands in $Sr_3(VO_4)_2$ in the (a) 1000–600 cm^{-1} and (b) 500–100 cm^{-1} frequency ranges and in $Ba_3(VO_4)_2$ in the (c) 1000–600 cm^{-1} and (d) 500–100 cm^{-1} frequency ranges. The open symbols represent compression data and the solid ones represent decompression data. The lines are guides for the eyes.

We suggest the following interpretation for the changes observed in the $Ba_3(VO_4)_2$ spectrum above approximately 120 kbar. Initially, the adjacent VO_4^{3-} groups in the intralayer sites are separated by 3.935 Å (V...V distance), and the

distance between one V atom and the O(2) (intralayer) oxygen of an adjacent VO_4^{3-} unit is 3.724 Å. Our Raman results indicate that compression below 100 kbar is mainly taken up by relative displacements of the interlayer cations,
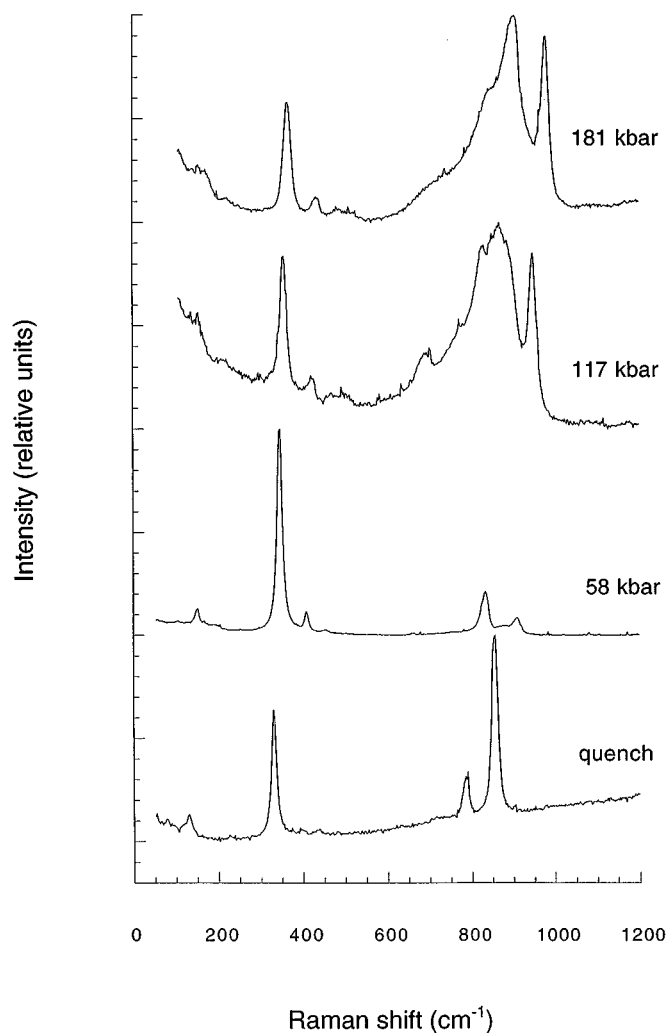
FIG. 6. Raman spectra of $Sr_3(VO_4)_2$ upon decompression.

FIG. 7. Raman spectra of $Ba_3(VO_4)_2$ upon decompression.

perhaps coupled with slight rotations or distortions of the vanadate units. At higher pressure, the mode of compression obviously changes, because of the large changes observed in the Raman spectra. It is quite possible that adjacent distorted VO_4^{3-} groups may be forced together sufficiently for condensation to occur *via* edge- or corner-sharing. A similar mechanism has been described for Mg_2SiO_4 and Mg_2GeO_4 olivines (20, 21), which have a related structure (Fig. 8). It is of interest that the broad but well-defined band in the spectrum of $Ba_3(VO_4)_2$ at high pressure occurs at 800 cm^{-1}, which the frequency observed for the high pressure phase of $LiVO_3$ in the $LiNbO_3$ structure, containing corner-linked VO_6 groups (12, 13). However, the structural change does not occur homogeneously throughout the sample, because the $Ba_3(VO_4)_2$ spectrum is still dominated by both the tetrahedral V–O stretching and the O–V–O bending modes of the ambient pressure orthovanadate phase (Figs. 4 and 7). The proposed vanadate condensation also occurs continuously along a structural coordinate, be-
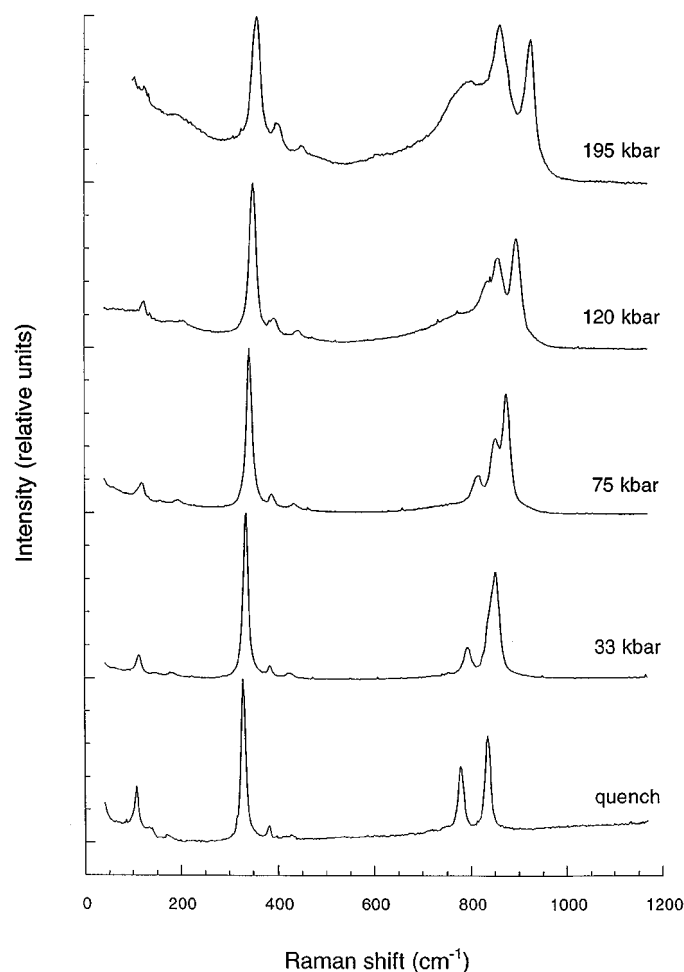
cause it is not associated with any significant hysteresis on decompression.

This model then aids in our interpretation of the qualitatively different observation for $Sr_3(VO_4)_2$. The orthovanadate condensation mechanism described for $Ba_3(VO_4)_2$ provides a low energy pathway for the ambient pressure structure, which is structurally related to olivine (Fig. 8), to transform to one of the family of spinelloids (23, 24). We have deduced an analogous structural change from the Raman spectrum and X-ray diffraction pattern of Mn_2SiSe_4, which has the olivine structure at ambient pressure (25). We propose that completion of this "reaction" is hindered in the case of $Ba_3(VO_4)_2$ because of the large size of the Ba^{2+} cations. However, the transformation can be completed (or nearly so) in the case of $Sr_3(VO_4)_2$, so that the spectrum at 207 kbar corresponds to that of a structurally heterogeneous mixture of spinelloid regions, presumably with different degrees of stacking coherence. This would explain the fact that the high pressure form of $Sr_3(VO_4)_2$, as evidenced by its Raman spectrum, exhibits a large hysteresis
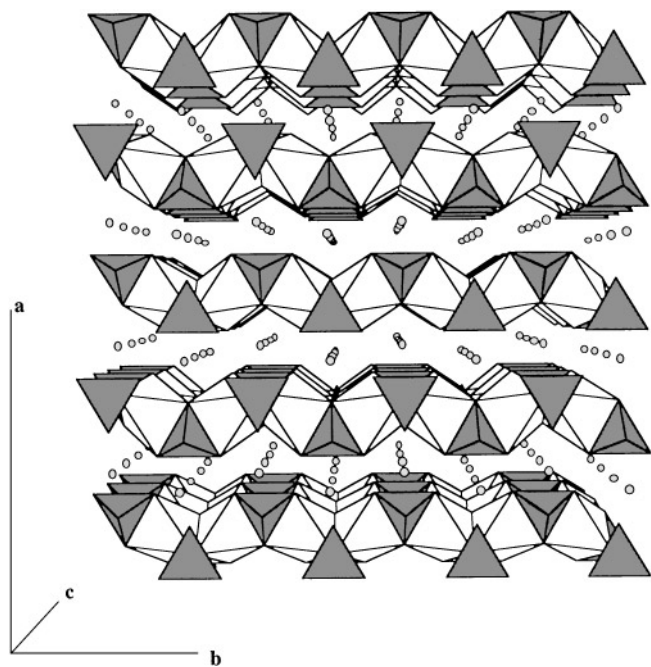
FIG. 8. The crystal structure of Mg_2SiO_4 olivine, *Pnma* space group (22). Both the $Me_{(1)}$ (C_i site symmetry) and $Me_{(2)}$ (C_s site symmetry) atoms are in sixfold distorted octahedral coordination. The tetrahedral units occupy the C_s sites. In the hypothetical case of $Me_3(XO_4)_2$ with that structure type, the vacancies ($\otimes$) are randomly distributed at the $Me_{(2)}^{2+}$ sites (filled circles), $Me_{(1)}(Me, \otimes)_{(2)}XO_4$. In both palmierite (see Fig. 1) and olivine structures, the oxygen atoms form a hexagonal close packing. The packing in the olivine structure is distorted from this due to loss of the three-fold axis.

(to 117 kbar) on decompression, consistent with the material having undergone a first order phase change into the spinelloid family of structures. It is worthwhile to note that, unlike the $Ba_3(VO_4)_2$ analog, the characteristic peaks of the low pressure structure have almost disappeared in the spectrum taken at 207 kbar (Fig. 3), although they are partly recovered on decompression to 117 kbar, and fully recover below this pressure (Fig. 6).

CONCLUSION

We have studied the Raman spectra of $Sr_3(VO_4)_2$ and $Ba_3(VO_4)_2$ at ambient conditions and *in situ* at high pressure. The results from compression to moderate pressures (below 75 kbar) permit the assignment of all of the high frequency modes associated with stretching and bending of the VO_4^{3-} groups, as well as most of the modes derived from the interlayer cation displacements and the vanadate librations and translations. The A_{1g} and E_g modes associated primarily with metal ion translations are assigned based on their shift with cation mass. On compression to above 95 kbar, distortions of the vanadate units or nonsymmetric displacements of the alkaline earth cations are revealed by a splitting of the E_g mode associated with V–O stretching

vibrations. At higher pressure, the spectra begin to change markedly in form, with appearance of new, broad bands in the high frequency region. In the case of $Ba_3(VO_4)_2$, these can be interpreted as being due to condensation of adjacent VO_4^{3-} units into edge- or corner-shared octahedra. Only a fraction of vanadate units within the structure participates in this structural change, which is fully reversible with little or no hysteresis on decompression. For the strontium compound, this process provides a relatively easy pathway for transformation into the spinelloid series of structures, accessed *via* a mechanism by which alternate V^{5+} ions pass through the triangular faces of their original distorted tetrahedral site, associated with aperiodic lattice translations (23, 24). Further investigations of these materials at high pressure will be required using X-ray diffraction to fully elucidate the mechanisms of the structural change. The first order phase change and associated hysteresis noted in $Sr_3(VO_4)_2$ is a promising result for obtaining new families of these materials by high pressure synthesis (12, 13).

REFERENCES

1. A. A. Fotiev, B. K. Trunov, and V. D. Zhuravlev, "Vanadates of Divalent Metals." Nauka, Moskva, 1985 [in Russian].
2. V. D. Zhuravlev, A. A. Fotiev, and B. V. Shulgin, *Izv. Akad. Nauk SSSR Neorg. Mater.* **15,** 2003 (1979).
3. L. D. Merkle, A. Pinto, H. Verdun, and B. McIntosh, *Appl. Phys. Lett.* **61,** 2386 (1992).
4. B. Buijsse, J. Schmidt, I. Y. Chan, and D. J. Singel, *Phys. Rev. B,* **51,** 6215 (1995).
5. V. D. Zhuravlev and A. A. Fotiev, *Zh. Neorg. Khimii* **25,** 2560 (1980).
6. L. V. Kristallov and A. A. Fotiev, *Zh. Neorg. Khimii* **26,** 2718 (1981).
7. P. Roux and G. Bonel, *Rev. Chim. Miner.* **22,** 767 (1985).
8. A. Durif, *Acta Crystallogr.* **12,** 420 (1959).
9. P. Tarte and I. Thelen, *Spectrochim. Acta A* **28,** 5 (1972).
10. E. J. Baran and P. J. Aymonino, *J. Mol. Struct.* **11,** 453 (1970).
11. W. Carrillo-Cabrera and H. G. von Schnering, *Z. Kristallogr.* **205,** 271 (1993).
12. A. Grzechnik and P. F. McMillan, *J. Phys. Chem. Solids* **59,** 159 (1995).
13. A. Grzechnik and P. F. McMillan, *J. Phys. Chem. Solids,* in press (1997).
14. K. Leinenweber, A. Grzechnik, M. Voorhees, A. Navrotsky, N. Yao, and P. F. McMillan, *Phys. Chem. Miner.,* in press (1997).
15. A. Grzechnik, R. Chamberlin, H. Hubert, P. F. McMillan, and A. Chizmeshya, *E. J. Inorg. Solid State Chem.,* in press (1997).
16. A. Grzechnik and P. F. McMillan, *Solid State Commun.,* in press (1997).
17. H. K. Mao, P. M. Bell, J. W. Shaner, and D. J. Steinberg, *J. Appl. Phys.* **49,** 3276 (1978).
18. H. G. Bachmann and W. Kleber, *Fortschr. Mineral.* **31/32,** 9 (1953).
19. P. Süsse and M. J. Buerger, *Z. Kristallogr.* **134,** 161 (1970).
20. D. J. Durben, P. F. McMillan, and G. H. Wolf, *Am. Miner.* **78,** 1143 (1993).
21. B. Reynard, P.-E. Petit, F. Guyot, and Ph. Gillet, *Phys. Chem. Miner.* **20,** 556 (1994).
22. R. W. G. Wyckoff, "Crystal Structures," 2nd ed., Vol. **3**. Robert E. Krieger, Malabar, 1981.
23. B. G. Hyde, T. J. White, M. O'Keeffe, and A. W. S. Johnson, *Z. Kristallogr.* **160,** 53 (1982).
24. M. O'Keeffe and B. G. Hyde, *Struct. Bonding* **61,** 77 (1985).
25. A. Grzechnik and P. F. McMillan, *J. Phys. Chem. Solids* **58,** 413 (1997).